Acta Pharmaceutica Sinica B 2026;16(8):5312−5327

Chinese Pharmaceutical Association
Institute of Materia Medica, Chinese Academy of Medical Sciences

Acta Pharmaceutica Sinica B

www.elsevier.com/locate/apsb
www.sciencedirect.com

ORIGINAL ARTICLE

Neutralizing dentin sialophosphoprotein facilitates tumor vascular normalization in colorectal cancer by blocking the crosstalk between tumor cells and endothelial cells

Chaoqun Liu[a,b,†], Rui Zhou[a,b,†], Weiwei Liu[a,b,†], Rui Li[a,b,†], Jun Xiao[a,b], Jianghua Wu[b], Ziyan Ning[b], Zilin Chen[b], Cheng Qian[b], Yujie Zhang[b], Wandie Lin[b], Liang Zhao[a,b,*]

[a]*Department of Pathology, Nanfang Hospital, Southern Medical University, Guangzhou 510515, China*
[b]*Department of Pathology & Guangdong Province Key Laboratory of Molecular Tumor Pathology, School of Basic Medical Sciences, Southern Medical University, Guangzhou 510515, China*

Received 12 April 2025; received in revised form 11 August 2025; accepted 9 September 2025

KEY WORDS

Colorectal cancer;
Metastasis;
Microenvironment;
Tumor vessel normalization;
DSPP;
Integrin $\alpha v\beta 3$;
MAPK pathway;
Interleukin-17 F

Abstract Irregular, curved, and uneven shapes of tumor vessels contribute to a malignant microenvironment, promoting metastasis. In this study, using patient-derived xenograft models, we observed that tumors derived from metastatic colorectal cancer (CRC) tissues exhibited increased vascular density, hypoxia, and permeability, but reduced perfusion and pericyte coverage, compared with tumors derived from non-metastatic CRC tissues. We conducted a high-throughput microarray analysis to determine the molecular mechanisms underlying compromised vessel structures. Dentin sialophosphoprotein (*DSPP*) was identified as the most upregulated gene in metastatic CRC with abnormal vasculature. Clinically, high *DSPP* expression is strongly correlated with poor prognosis and advanced CRC stages. DSPP stimulates tumor vessel abnormalization and CRC metastasis *in vivo*, and acts as a novel ligand of alpha(v)beta (3) integrin ($\alpha v\beta 3$), which is predominantly expressed in tumor vessels. DSPP could directly bind to the peptide segment (amino acids 368−411) of $\alpha v\beta 3$ on the cytoplasmic membrane of endothelial cells, activating the mitogen-activated protein kinase signaling pathway. Subsequently, therapeutic targeting of DSPP with human DSPP antibody or TFA, a selective inhibitor of the $\alpha v\beta 3$, was investigated to effectively induce tumor vessel normalization and suppress tumor metastasis in mice. Additionally, interleukin-17 F (IL-17F) was identified as an upstream regulator of *DSPP* expression, which promotes

*Corresponding author.
E-mail address: liangsmu@foxmail.com (Liang Zhao).
†These authors made equal contributions to this work.
Peer review under the responsibility of Chinese Pharmaceutical Association and Institute of Materia Medica, Chinese Academy of Medical Sciences.

https://doi.org/10.1016/j.apsb.2026.06.011

DSPP transcription *via* p65 binding to its promoter. Therefore, targeting the DSPP/$\alpha v\beta 3$ axis to promote tumor vessel normalization and inhibit tumor metastasis represents a new strategy for the clinical implementation of combination targeted therapies in patients with advanced CRC.

1. Introduction

Colorectal cancer (CRC) is the third most common cancer worldwide and the leading cause of cancer-related mortality in individuals aged <50 years[1]. Despite advances in treatment, CRC-related mortality, particularly from metastatic CRC (mCRC), remains high[2,3]. Approximately 20% of patients are diagnosed with mCRC at the outset, and a significant proportion of individuals experience disease progression to metastatic stage[2,3]. Determining the molecular mechanisms underlying mCRC is crucial to improving tumor treatment strategies. Blood vessels within tumors play a significant role in metastasis and invasion. Targeting tumor vessels at the molecular level, such as through a combination of anti-vascular endothelial growth factor therapy and chemotherapy, is a more effective therapeutic strategy for patients with mCRC[4]. Exploring the association between tumor vessels and the malignant behavior of CRC and identifying new molecular targets are essential for the optimization and development of intervention strategies for CRC[5−9].

Tumor blood vessels often exhibit structural and functional abnormalities compared with the normal blood vessels[5,9]. Furthermore, tumor blood vessels exhibit irregular shapes and sizes, tortuous structures, and considerable morphological heterogeneity. Specifically, hypoxic conditions enhance the aggressiveness of cancer cells, whereas permeable blood vessels facilitate their migration and metastasis to remote locations[10]. The leaky endothelial cell (EC) barrier and reduced pericyte attachment to tumor vessels facilitate the intravasation and dissemination of cancer cells. Strategies to normalize tumor vessels aim to reduce metastasis and enhance chemotherapy efficacy by restoring proper perfusion, in addition to depriving cancer cells of nutrients by preventing angiogenesis and damaging existing tumor vessels[11−13]. A low dose of bevacizumab could induce tumor vessel normalization (TVN), reduce hypoxia, and potentiate cancer immunotherapy[14,15]. However, the functional mechanisms underlying the compromised vessel structures remain unclear. Investigating the relationship between tumor vasculature and the aggressive characteristics of CRC is crucial for advancing early intervention aimed at TVN.

The small integrin-binding ligand N-linked glycoproteins (SIBLINGs), including osteopontin (OPN), bone sialoprotein (BSP), dentin matrix protein-1 (DMP1), dentin sialophosphoprotein (DSPP), and matrix extracellular phosphoglycoprotein (MEPE), are crucial for various biological processes involved in tumor progression. These molecules play important roles in tumor cell adhesion, proliferation, invasion, angiogenesis, and metastasis by interacting with specific cell surface receptors, including integrins (which engage *via* arginine−glycine−aspartic (RGD) and non-RGD motifs) and CD44[16,17].

DSPP is mainly known for its role in dentin formation[18−20], but emerging research suggests it may also play a role in cancer biology across various tumor types. DSPP contributes to the aggressive behavior of cancer cells by influencing cell adhesion, metastasis, angiogenesis, cancer cell stemness, and epithelial−mesenchymal transition[21−25]. Notably, DSPP is a prostate cancer biomarker correlated with tumor aggressiveness[26−28]. Nevertheless, its involvement in the mCRC remains debatable.

In contrast to conventional vessel normalization approaches typically aimed at identifying target genes within the endothelial layer, basement membrane, and mural cells, this study explored a novel biomarker in CRC cells with significant relevance to abnormal tumor vasculature.

2. Materials and methods

2.1. Human CRC samples

Primary CRC samples, matched non-cancerous colorectal tissues, and paraffin-embedded biopsy specimens from patients with CRC were obtained from the tumor tissue bank. Clinical and long-term follow-up data from 174 patients with CRC collected from January 2010 to June 2021 were analyzed. None of the patients received any local or systemic anticancer therapy before radical surgery. This study was approved by the Biomedical Research Ethics Committee of Nanfang Hospital (No. NFEC-2021-431), and informed consent was obtained from all patients.

2.2. Cell lines and cell culture

CRC and normal colon epithelial cell lines were obtained from the Cell Bank of the Chinese Academy of Sciences. All cells were cultured in RPMI-1640 medium (HyClone, Cleveland, OH, USA) enriched with fetal bovine serum (FBS, Gibco, Thermo Fisher Scientific, Waltham, MA, USA) as previously described[29]. HUVEC and 293 T cells were kindly gifted by Dr. Li Qin at the Baylor College of Medicine. These cells were cultured in DMEM/high-glucose medium (HyClone) enriched with FBS. Inhibitors, including the mitogen-activated protein kinase (MAPK) kinase inhibitor selumetinib (AZD6244, MCE, Monmouth Junction, NJ, USA) or cyclo (-RGDfK) TFA (HY-P0023A, MCE), were introduced into the cultured cells. All cells were incubated in a controlled environment at 37 °C with 5% CO_2 in a humidified atmosphere.

2.3. Patient-derived xenograft (PDX) model

The CRC PDX model was established as previously described[29]. Briefly, fresh CRC tumor tissues were finely cut into 3 mm × 3 mm × 3 mm blocks on ice using sterile scissors and a scalpel. The non-necrotic fragments were then isolated carefully. A 5 mm incision was made in the upper abdomen of non-obese

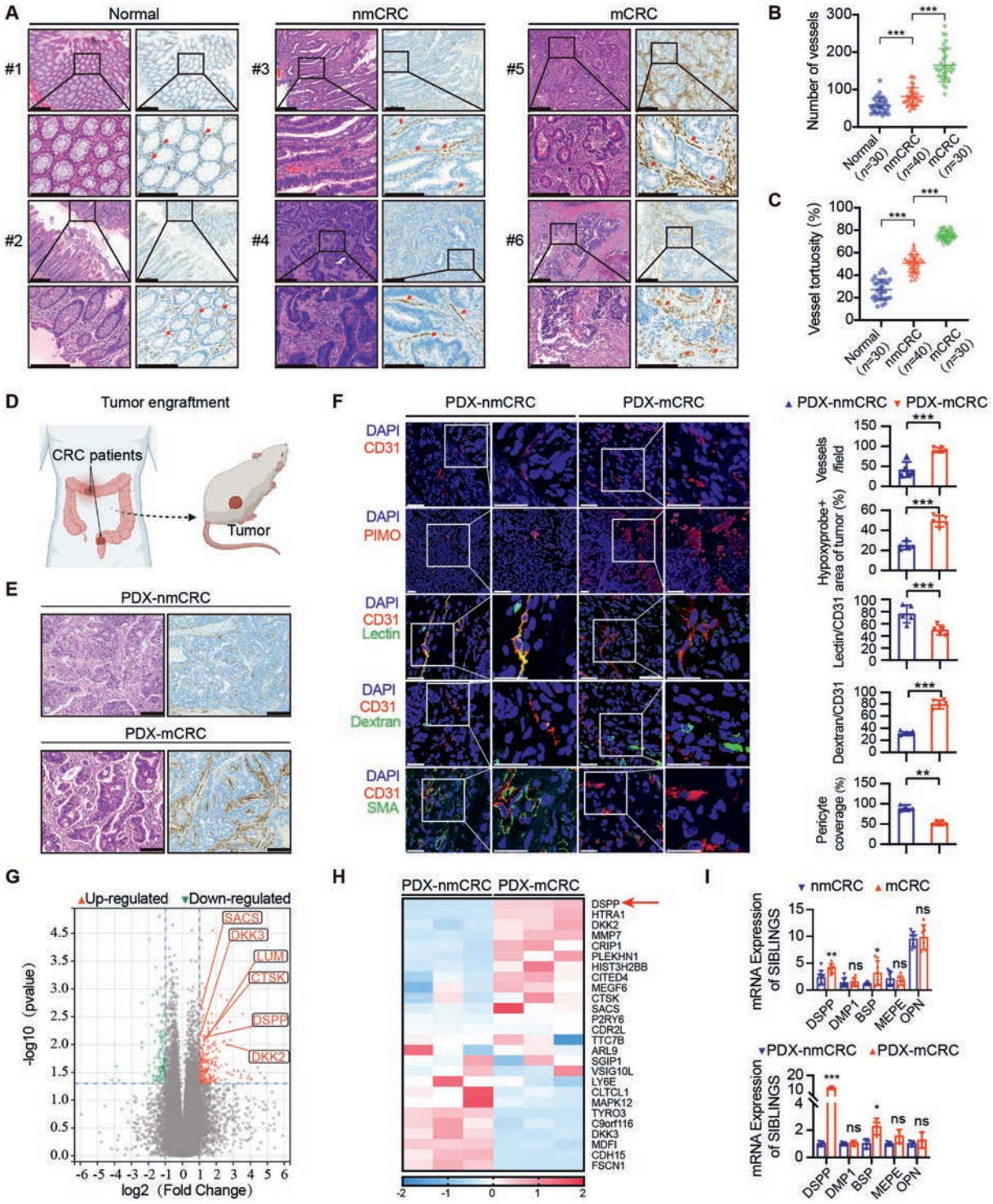

Figure 1 Vascular morphology in CRC and screening of target genes related to abnormal vessels. (A) Representative images of hematoxylin and eosin (HE) and Immunohistochemistry (IHC) staining of CD31 in clinical colorectal cancer (CRC) tissues. (B, C) Quantification of tumor blood vessels and tortuous vessels in CRC tissues and adjacent normal mucosal tissues. (D) Schematic of the CRC patient-derived xenograft (PDX) model construction. (E) HE and IHC staining of PDX tumors. (F) PDX tumors were immunostained to assess blood vascular density, hypoxia, vascular perfusion, vessel permeability, and α-SMA$^+$ pericyte coverage ($n = 5$). (G) Volcano plot depicting differentially expressed genes identified from a high-throughput microarray dataset involving eight pairs of metastatic and non-metastatic human CRC tissues (NCBI/GEO/GSE113296). (H) Heat map of 26 differentially overexpressed genes in PDX mice with normal/abnormal tumor vessels. (I) Transcriptional expression of *DSPP*, *DMP1*, *BSP*, *MEPE*, and *OPN* in the high-throughput microarray datasets and PDX tumors. Data are presented as mean ± SD. $^*P < 0.05$, $^{**}P < 0.01$, $^{***}P < 0.001$; ns, no significance. Scale bars = 100 μm.

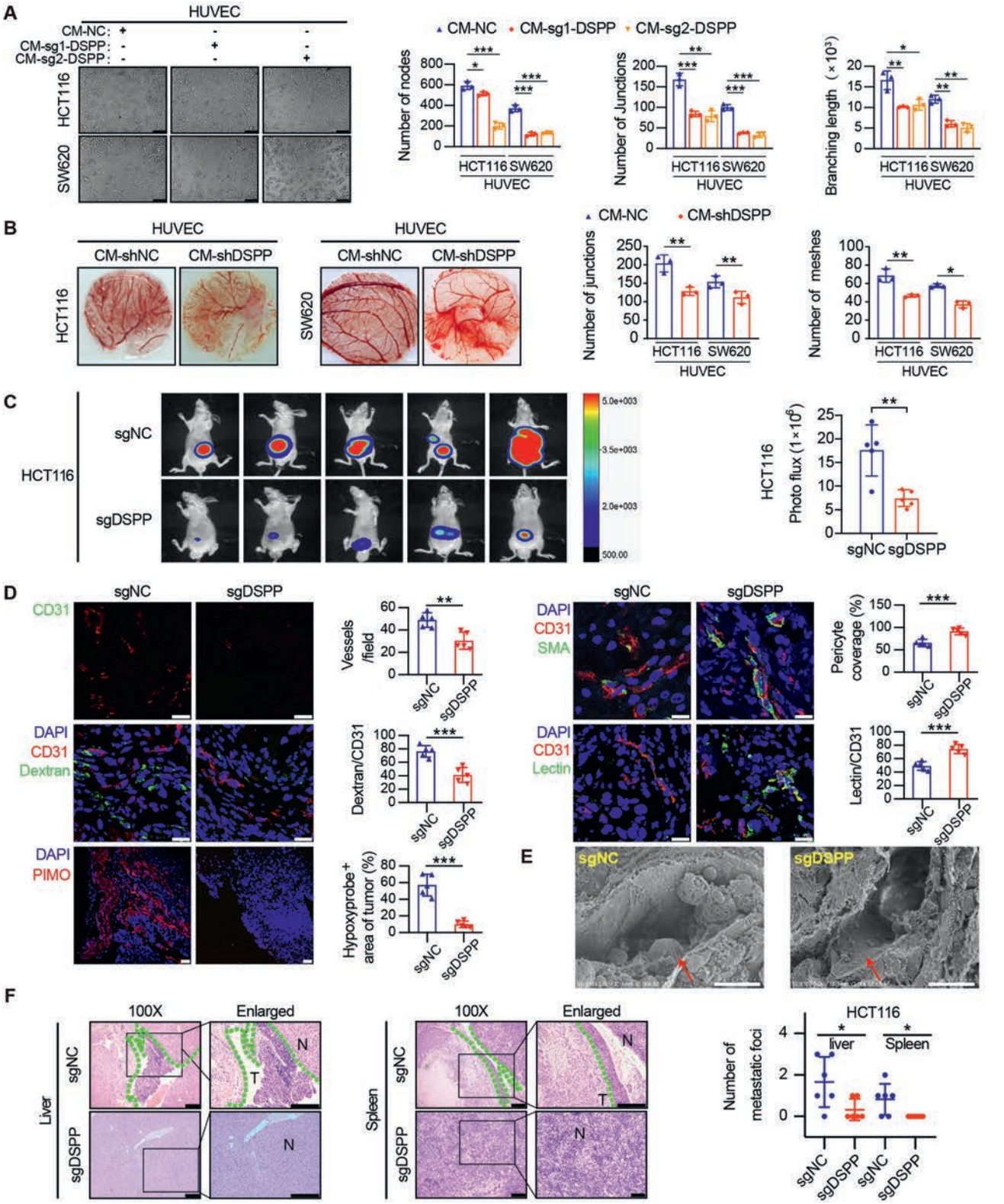

Figure 2 CRC cell-secreted DSPP induces tumor angiogenesis to promote tumor vascular abnormality and metastasis. (A) Representative tubular structures formed by HUVECs treated with indicated conditioned media (CM) from HCT116 and SW620 cells. Bars on the right represent the number of capillary tubule nodes and junctions, and the branching length. Data are presented as mean ± SD ($n = 3$). (B) Representative images of blood vessels formed in CAM assays following treatment with CM from the indicated HCT116 and SW620 cell lines. The bars on the right illustrate the number of blood vessel junctions and meshes. Data are presented as mean ± SD ($n = 3$). (C) Representative *in vivo* bioluminescent images of orthotopic tumor-bearing mice transplanted with the indicated HCT116 cells. The fluorescence signal intensities of tumors are shown on the right. Data are presented as mean ± SD ($n = 5$). (D) Immunofluorescence (IF) staining images showing $CD31^+$ blood vessel (BV) density, $hypoxyprobe^+$ areas, SMA^+ pericyte coverage, dextran leakage, and lectin perfusion in tumor vessels in orthotopic tumors derived from indicated cells. Scale bars = 40 μm. Data are presented as mean ± SD ($n = 5$). (E) Scanning electron microscopy images showing tumor vessels derived from control and *sgDSPP* HCT116 cells. (F) HE staining was used to observe tumor metastasis in the liver and spleen. $^*P < 0.05$, $^{**}P < 0.01$, $^{***}P < 0.001$; ns, no significance.

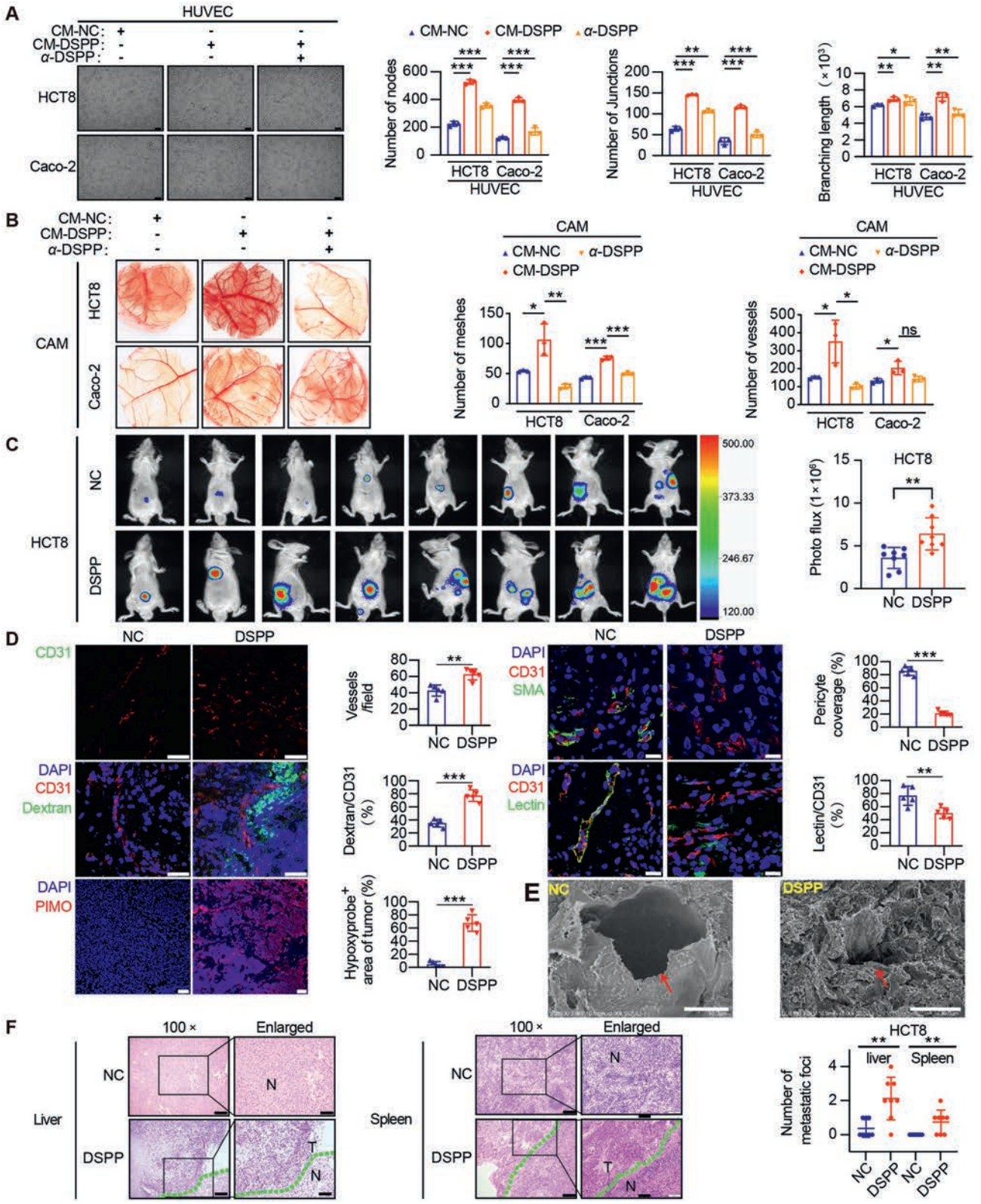

Figure 3 Inhibition of DSPP secretion reduces angiogenesis, vascular abnormalities, and metastasis of CRC. (A) Representative tubular structures formed by HUVECs treated with CM from indicated HCT8 and Caco-2 cells. The number of capillary tubule nodes and junctions, and the branching length are shown on the right. Scale bars = 100 μm. Data are presented as mean ± SD (n = 3). (B) Representative images illustrating blood vessel formation in the chorioallantoic membrane (CAM) assay following treatment with CM from indicated HCT8 and Caco-2 cells. The number of the blood vessel junctions and meshes is shown on the right. Data are presented as mean ± SD (n = 3). (C) Representative images of orthotopic tumor-bearing mice transplanted with the indicated HCT8 cells. The fluorescence signal intensities of tumors are shown on

diabetic severe combined immunodeficiency mice, and tumor blocks were implanted into the incision site.

2.4. Pimonidazole staining and blood vessel leakiness analysis

Mice were intravenously injected with 2 mg of hypoxyprobe 20 min before tumor resection to allow circulation and hypoxia analysis. Subsequently, tumor sections were stained using the Hypoxyprobe Plus Kit (HP2, Hypoxyprobe, Burlington, VT, USA) following the manufacturer's instructions. Mice were administered 1 mg of 50 μg fluorescein-labeled lycopersicon esculentum (tomato) lectin (FL-1171, Vectorlabs, Newark, CA, USA) and 70 kDa fluorescein-labeled dextran (MS0905, MKBio, Shanghai, China) to assess vessel leakiness. Whole-animal perfusion fixation was performed as described for the Evans Blue assay after 10 min. The tumors were then carefully removed, fixed in 4% paraformaldehyde overnight, and either frozen or embedded in paraffin for subsequent analyses. All animal experiments were approved by the Institutional Animal Ethics Committee of the Southern Medical University Laboratory Animal Center (No. SMUL202310034), and conducted in accordance with its guidelines.

2.5. Culture of tumor organoids derived from patients with CRC

Patient-derived tumor organoids (PDTOs) were established using human CRC tissues as described previously[30,31]. Briefly, fresh tissues from patients with colon adenocarcinoma were mechanically disrupted using a gentle cell dissociation reagent (07174, STEAMCELL, Vancouver, Canada) and then filtered through a 70 μm mesh. The filtered samples were centrifuged at 300 × *g* for 5 min and mixed with Matrigel (356231, Corning, New York, NY, USA). The mixture was then seeded into 24-well plates, and the culture medium (K2103-CR, bioGenous, Beijing, China) was refreshed every 2 days. Organoids were dissociated using an organoid dissociation solution (E238001, bioGenous) and passaged every 7−14 days. PDTOs were gene-edited as previously described[30]. Virus particles were resuspended in organoid culture medium containing 8 μg/mL polybrene (Merck KGaA, Darmstadt, Germany) and incubated with the organoids for 4 h. Thereafter, organoids were embedded in Matrigel and cultured in medium containing 10 μmol/L Y-27632 (S6390, Selleck, Houston, TX, USA). Approximately 48 h after viral infection, organoids were selected for seven consecutive days in medium containing 2 μg/mL puromycin.

2.6. Fixation and embedding of PDTOs

After PDTOs reached 80%−90% confluence in a 24-well plate, the culture medium was removed, and 1 mL of cold 4% paraformaldehyde was added for fixation for 1 h. The organoids were gently placed into a 15 mL centrifuge tube and incubated in 10 mL of cold phosphate-buffered saline for 10 min. PDTOs were then precipitated with 2%−5% molten agarose to form agarose blocks, which were dehydrated and cleared before paraffin embedding. Finally, 3 μm paraffin sections were prepared for the subsequent experiments.

2.7. Glutathione sulfhydryl transferase (GST) pull-down assay

The coding sequences of integrin subunit alpha V (*ITGAV*) (1−438 amino acids) and integrin subunit beta 3 (*ITGB3)* (109−352 amino acids) were cloned into pGEX-4T-1 vectors containing a GST-tagged open reading frame. The recombinant plasmids GST-ITGAV-aa1−438 and GST-ITGB3-aa109−352 were transformed into *Escherichia coli* BL21 (DE3). GST or GST fusion protein expression was induced using IPTG when the cell density reached approximately 60%. After harvesting, the cell pellet was resuspended in phosphate-buffered saline supplemented with a protease inhibitor cocktail and PMSF and subjected to ultrasonic fracturing. The supernatant was collected and incubated with glutathione Sepharose in a rotating incubator at 4 °C overnight. Subsequently, the purified GST-fusion protein or the GST control was mixed with the cell lysates of HEK293T cells transfected with the FLAG-DSPP plasmid and incubated together at 4 °C overnight. Protein complexes bound to the beads were washed off and subsequently detected using Western blotting.

2.8. Statistical analysis

The SPSS version 19.0 software (SPSS, Chicago, USA) was utilized to perform data analysis. Nonparametric tests and Kaplan-Meier survival analysis were employed to analyze the clinical data. Pearson's chi-squared (χ^2) test and Student's *t*-test were used to evaluate the significance of differences among diverse groups. All statistical tests conducted were two-sided. The mean values ± standard deviation (SD) were presented in the data format. The *P*-values are depicted in the figures ($^{\#}P > 0.05$, $^{*}P < 0.05$, $^{**}P < 0.01$, $^{***}P < 0.001$).

3. Results

3.1. Vascular morphology in CRC and screening of target genes related to abnormal vessels

The primary CRC tissues from patients with metastasis (mCRC) exhibited a considerably higher number of tortuous blood vessels and a deficiency of pericytes compared with primary CRC tissues from non-metastatic patients (nmCRC) (Fig. 1A−C and Supporting Information Fig. S1A). Regarding the structure and functional properties of tumor vessels in PDX models of CRC (Fig. 1D), vessels of PDX tumors derived from mCRC tissues (PDX-mCRC) exhibited an increased blood vascular density, hypoxia, and permeability, and decreased vascular perfusion and α-smooth muscle actin (α-SMA$^+$) pericyte coverage compared with the PDX tumors derived from nmCRC tissues (PDX-nmCRC, Fig. 1E and F).

We identified 26 upregulated genes in the mCRC samples in a previously published high-throughput microarray dataset (NCBI/GEO/GSE113296) involving eight paired samples of non-

the right. Data are presented as mean ± SD ($n = 8$). (D) IF staining images showing the CD31$^+$ blood vessel (BV) density, hypoxyprobe$^+$ areas, SMA$^+$ pericyte coverage, dextran leakage, and lectin perfusion in tumor vessels in orthotopic tumors derived from indicated cells. Data are presented as mean ± SD ($n = 5$). Scale bars = 40 μm. (E) Scanning electron microscopy showing tumor vessels derived from control and HCT8 cells with *DSPP* overexpression. (F) The HE analysis was used to observe the metastasis of orthotopic tumors in the liver and spleen. $^{*}P < 0.05$, $^{**}P < 0.01$, $^{***}P < 0.001$; ns, no significance.

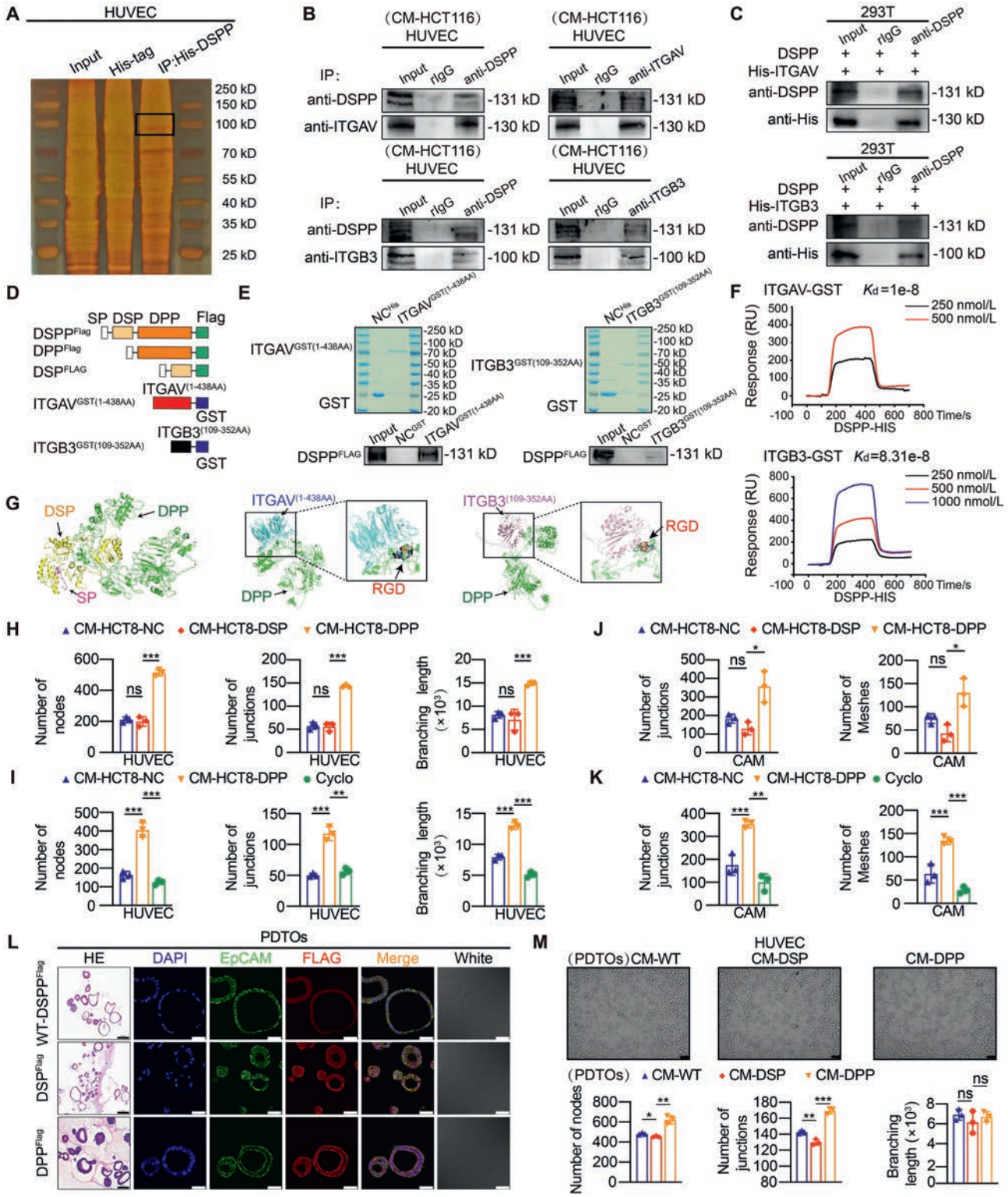

Figure 4 DSPP directly interacts with integrin $\alpha v\beta 3$. (A) The silver staining result shows the differential expression bands of DSPP-interacting proteins after the IP assay. (B) The interaction between DSPP and integrin subunit alpha V (ITGAV) and integrin subunit beta 3 (ITGB3) in CM-treated HCT116 cells was investigated by co-immunoprecipitation (Co-IP) assays. (C) The interaction between DSPP and ITGAV/ITGB3 in 293 T cells was investigated by Co-IP assays. (D) Schematic diagram showing the truncation variants of Flag-DSPP, GST-ITGAV$^{AA1\text{-}438}$, and GST-ITGB3$^{AA109\text{-}352}$. (E) Glutathione sulfhydryl transferase (GST) pull-down assay demonstrating the direct binding of DSPP with ITGAV$^{AA1\text{-}438}$ and ITGB3$^{AA109\text{-}352}$. (F) The surface plasmon resonance was conducted to measure the binding affinity between DSPP and ITGAV/ITGB3. (G) The molecular docking model of DSPP and ITGAV/ITGB3 was performed by a docking program ZDOCK. (H, I) The quantification of capillary tubule nodes, junctions, and branching length of tubules formed by HUVECs treated with CM from indicated HCT8 cells. Data are presented as

metastatic and metastatic human CRC tissues (Fig. 1G). We determined the mRNA expression of these genes in PDX tumors. Notably, *DSPP* was the most significantly upregulated gene in PDX-mCRC tumors with abnormal vessels (Fig. 1H). As DSPP belongs to the SIBLINGs, we also detected the transcriptional expression of the other four SIBLINGs in high-throughput microarray datasets and PDX tumors. *DSPP* was the most significantly upregulated among all SIBLINGs (Fig. 1I). *DSPP* mRNA expression was assessed in 10 paired CRC samples and corresponding adjacent normal tissue samples (Fig. S1B). A significantly higher *DSPP* expression was observed in CRC tissues.

3.2. CRC cell-secreted DSPP induces tumor angiogenesis to promote tumor vascular abnormality and metastasis

We investigated *DSPP* expression in normal colon and CRC cell lines. *DSPP* expression was elevated in HTC116, SW620, and SW480 CRC cells at the translational level, whereas it was reduced in HCT8, DLD-1, and Caco-2 cells compared with that in the normal human colon epithelial NCM460 cells (Supporting Information Fig. S2A). Subsequently, we introduced a *DSPP* silencing vector (*shDSPP*) and two small guide RNAs (sgRNAs; sg*DSPP1* and sg*DSPP2*) into the HCT116 and SW620 cells (Fig. S2B and S2C and Supporting Information Table S1) to reduce its expression. Next, *DSPP* levels in conditioned media (CM) of NCM460 and various CRC cell lines were measured (Fig. S2D and S2E). DSPP expression in HCT116, SW620, and HUVEC cells was detected *via* immunofluorescence (Fig. S2F) and Western blot analyses (Fig. S2G). Consistently, DSPP was predominantly expressed in CRC cells.

DSPP knockdown in CRC cells significantly suppressed tubule formation in HUVECs and angiogenesis in the chicken chorioallantoic membrane (CAM) assay (Fig. 2A and B). Subsequently, we orthotopically implanted control and *sgDSPP* HCT116 cells into nude mice to further confirm the effects of DSPP on angiogenesis *in vivo* (Fig. 2C). The tumor vasculature analysis revealed reduced vascular density, permeability, and hypoxia and enhanced vascular perfusion and α-smooth muscle actin (α-SMA$^+$) pericyte coverage following *sgDSPP* silencing. Therefore, *DSPP* silencing affected the structure and function of tumor blood vessels (Fig. 2D). Scanning electron microscopy of the *sgDSPP*-treated group demonstrated a regular, smooth monolayer of endothelial cells (Fig. 2E). Furthermore, HE staining revealed smaller primary tumors with fewer liver and spleen metastatic foci in the sg*DSPP* group than in the control group (Fig. 2F and Fig. S2H). Moreover, the sg*DSPP* group exhibited longer overall survival in the survival analysis (Fig. S2I).

3.3. Inhibition of DSPP secretion reduces angiogenesis, vascular abnormalities, and metastasis of CRC

By transfecting *pEnter-DSPP* into HCT8 and Caco-2 cells, we generated two CRC cell lines overexpressing *DSPP* (Supporting Information Fig. S3A and S3B). The CM of *DSPP*-overexpressing CRC cells significantly increased tubule formation in HUVECs and angiogenesis in the CAM assay. These stimulatory effects on angiogenesis were dramatically inhibited by human DSPP antibody (α-DSPP) (Fig. 3A and B). In the orthotopically implanted nude mice model (Fig. 3C), *DSPP* overexpression could increase the blood vascular density, vascular permeability, and hypoxia and decrease vascular perfusion and α-SMA$^+$ pericyte coverage of tumor vessels (Fig. 3D). Scanning electron microscopy demonstrated irregular and chaotically organized EC lining in vessels of the primary tumors derived from the *DSPP* overexpressing CRC cells (Fig. 3E). The *DSPP*-overexpressing group exhibited larger primary tumors and more extensive liver and spleen metastases than the controls, suggesting that DSPP enhances tumor growth and metastatic (Fig. 3F and Fig. S3C). Furthermore, the *DSPP* overexpression group exhibited a shorter overall survival in the survival analysis (Fig. S3D).

3.4. DSPP directly interacts with integrin $\alpha v\beta 3$

An immunoprecipitation assay was performed to identify proteins that interact with DSPP. Proteins with a distinct band of the size approximately 100 kDa were examined using liquid chromatography-mass spectrometry (LC−MS/MS) (Fig. 4A). Subsequently, ITGAV, which encodes the αv subunit of the heterodimeric integrin $\alpha v\beta 3$ (alongside ITGB3 encoding the $\beta 3$ subunit), was identified as a DSPP-interacting protein (Supporting Information Fig. S4A). Moreover, analysis of the GSE118904 dataset revealed elevated expressions of *ITGAV* and *ITGB3* in vascular endothelial cells (Fig. S4B). Subsequently, the interactions between His-DSPP secreted by the CRC cells and ITGAV/ITGB3 receptors on HUVECs were investigated (Fig. 4B and C). Additionally, immunofluorescence assays confirmed a notable co-localization of DSPP and $\alpha v\beta 3$ on the HUVEC cell membrane (Fig. S4C).

As DSPP contains a specific RGD peptide sequence that could bind to the cytoplasmic membrane surface of $\alpha v\beta 3$, we constructed 2 GST-tagged $\alpha v\beta 3$ truncators containing two different extracellular domains defined as ITGAV-aa1−438 and ITGB3-aa109−352, respectively (Fig. 4D). The GST pull-down assay showed that FLAG-tagged DSPP could directly bind to ITGAV-aa1−438 and ITGB3-aa109−352 but not to the GST control (Fig. 4E). The surface plasmon resonance (SPR) assay was employed to measure the binding affinity between DSPP and $\alpha v\beta 3$ (Fig. 4F). Subsequently, we transduced HUVEC cells with small guide RNAs targeting *ITGAV* and *ITGB3* (sg*ITGAV* and sg*ITGB3*, respectively) to individually knock down the expression of αv and $\beta 3$ integrin subunits (Fig. S4D and Table S1). Notably, the pro-angiogenic effects of CM derived from *DSPP* overexpressing CRC cells were markedly attenuated in HUVEC cells with *ITGAV* or *ITGB3* knockout (Fig. S4E). Based on the protein function database Uniprot (https://www.uniprot.org) and literature reports, we found that DSPP functions by being cleaved into dentin sialoprotein (DSP) and dentin phosphoprotein (DPP), and the RGD sequence is located in the DPP. We predicted DPP−ITGAV (1−438 amino acids) and DPP−ITGB3 (109−352 amino acids) structures using I-TASSER and Phyre 2 software. Additionally,

mean ± SD ($n = 3$). (J, K) The number of the blood vessel junctions and meshes in CAM assays. Data are presented as mean ± SD ($n = 3$). (L) Representative HE staining images of patient-derived tumor organoids (PDTOs) are shown. Scale bars = 100 μm. IF assay confirming the successful construction of DSP/DPP overexpression PDTOs. Scale bars = 40 μm in IF images. (M) Representative tubular structures formed by HUVECs treated with indicated CM from indicated PDTOs. Scale bars = 100 μm. The lower panel shows the quantification of capillary tubule nodes, junctions, and branching length. Data are presented as mean ± SD ($n = 3$). *$P < 0.05$, **$P < 0.01$, ***$P < 0.001$; ns, no significance.

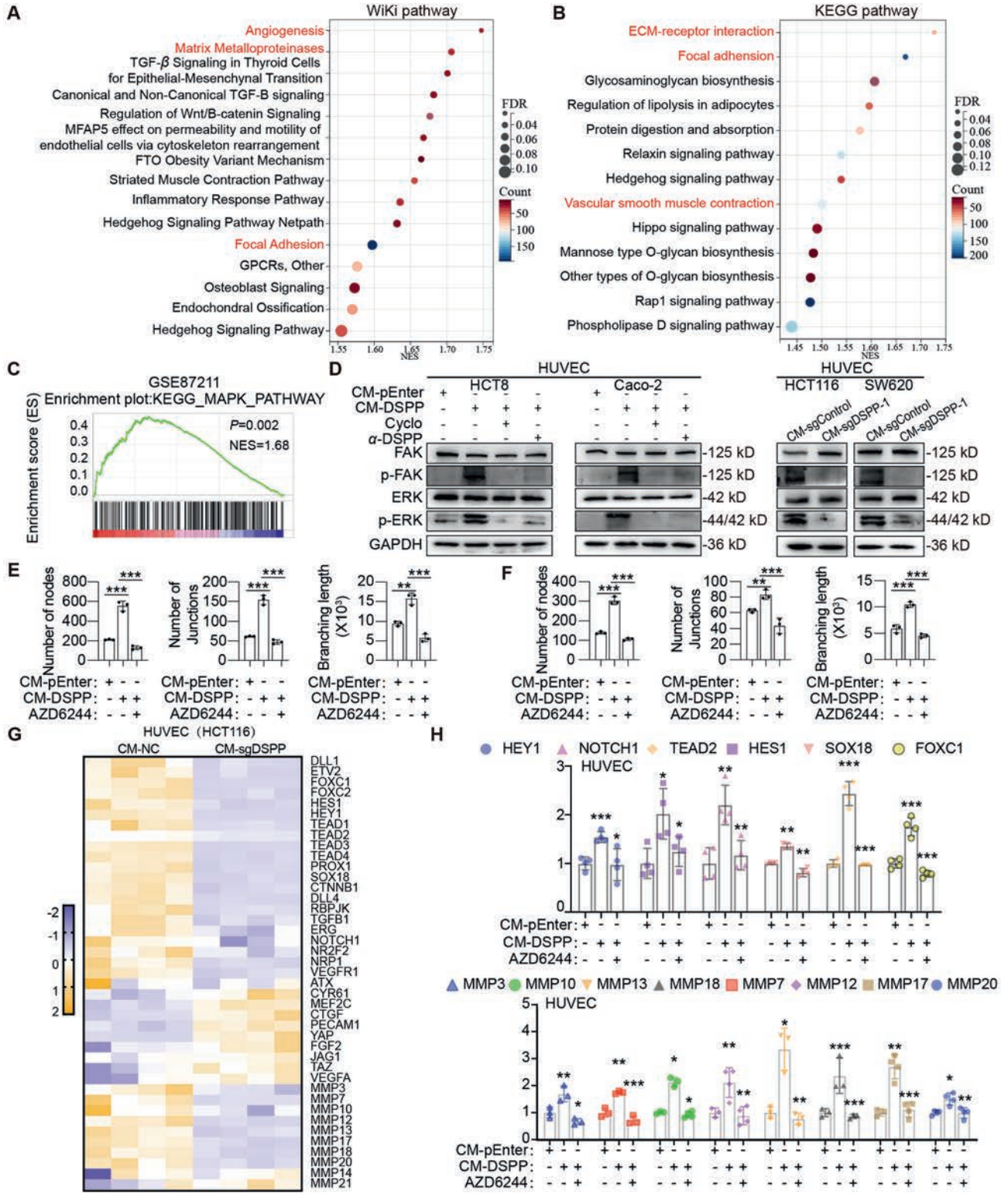

Figure 5 DSPP/αvβ3/MAPK signaling axis promotes tumor vessel abnormalization. (A, B) Investigating the potential regulatory functions of DSPP in CRC by the WiKi (A) and KEGG (B) pathway enrichment analysis. (C) The mitogen-activated protein kinase (MAPK)-related pathways were enriched in CRC with high *DSPP* expression by GSEA analysis. (D) Western blot assays showing the expression of the FAK/ERK pathway components in HUVEC treated with CM from the indicated CRC cells (E, F) Representative tubular structures formed by HUVECs treated with indicated CM from indicated HCT8/Caco-2 cells. Data are presented as mean ± SD ($n = 3$). (G) Heat map demonstrates the differentially expressed genes related to angiogenesis and matrix metalloproteinase family in HUVEC treated with CM from control and sg*DSPP* HCT116 cells. (H) Detecting the effect of AZD6244 on the DSPP-upregulated expression of angiogenesis and matrix metalloproteinase family-related genes by real-time quantitative PCR. Data are presented as mean ± SD ($n = 4$). $^{*}P < 0.05$, $^{**}P < 0.01$, $^{***}P < 0.001$.

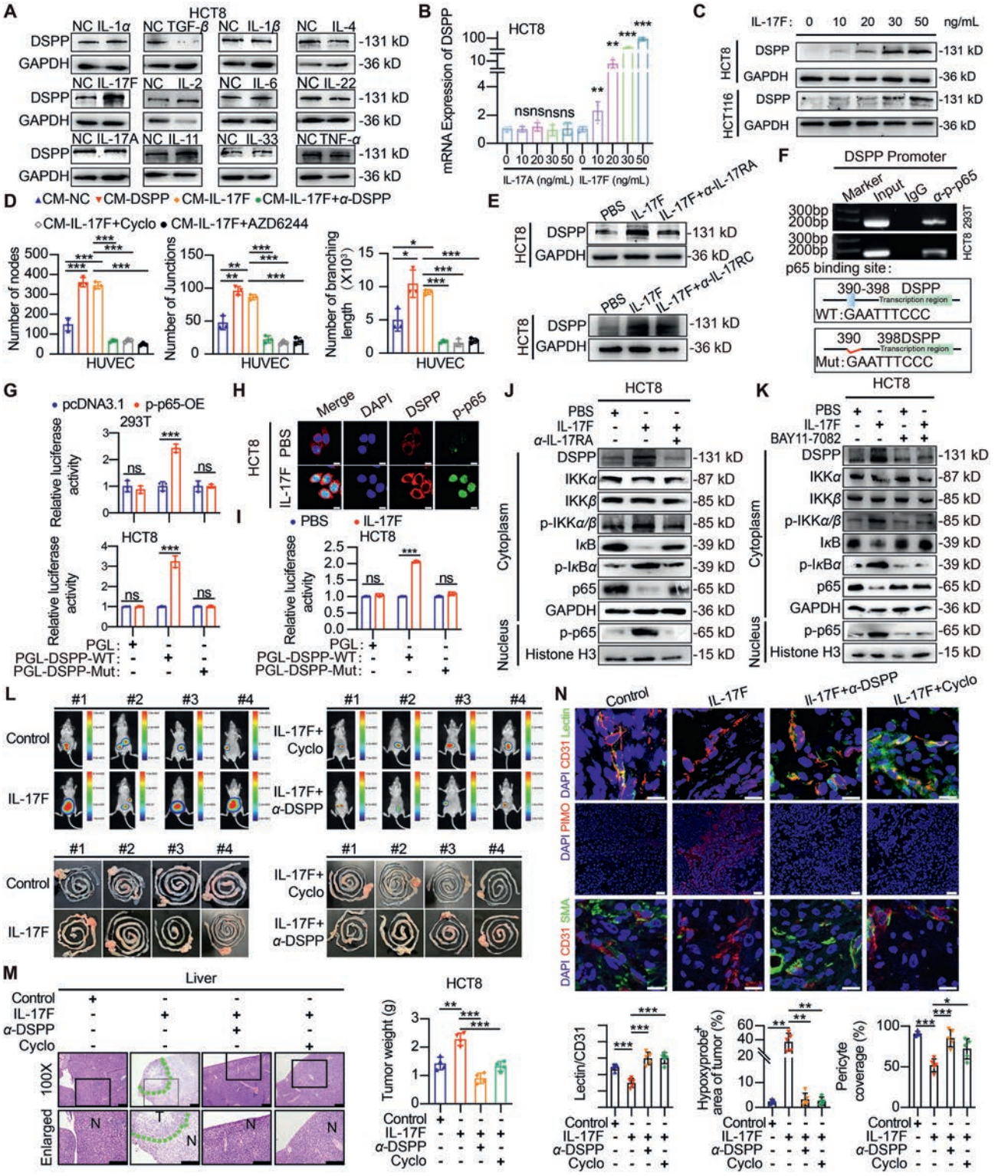

Figure 6 Interleukin (IL)-17F upregulates DSPP expression and induces vascular abnormalities in CRC. (A) Western blot assays show the DSPP expression in HCT8 cells stimulated with a series of relevant inflammatory factors. (B, C) Real-time qPCR, Western blot assays show the effect of IL-17F and IL-17A on the *DSPP* expression in HCT8 cells. (D) The quantification of capillary tubule nodes, junctions, and branching length was performed on HUVECs exposed to CM from HCT8 cells treated with DSPP antibody (α-DSPP), Cyclo(-RGDfK), and AZD6244. Data are presented as mean ± SD ($n = 3$). (E) Western blot analysis demonstrates the impact of the interleukin-17 receptor A/interleukin-17 receptor C antibody on DSPP expression induced by IL-17F in HCT8 cells. (F) Chromatin immunoprecipitation assays verified the location of the p65 binding site within the promoter region of *DSPP*. (G) Luciferase reporter assay demonstrates the direct interaction of p65 with the promoter region of *DSPP*. (H) IF staining shows an increased phosphorylation of intracellular p65 in IL-17F-stimulated HCT8 cells. Scale bars = 10 μm. (I)

ZDOCK was used to generate an interaction model between the two proteins (Fig. 4G). We successfully established FLAG-tagged *DSP*- and *DPP*-overexpressing CRC cell lines (Supporting Information Fig. S5B). Only the CM of CRC cells overexpressing *DPP* significantly enhanced tubule formation in HUVECs and promoted angiogenesis in the CAM assay (Fig. 4H and J and Fig. S5C and S5D). Therefore, CRC cell-derived DSPP induced angiogenesis mainly through the interaction between the translationally cleaved DPP protein and integrin $\alpha v\beta 3$ through its RGD sequence (Fig. 4I and K and Fig. S5E and S5F). Cyclo (-RGDfK) is a small-molecule inhibitor that specifically blocks $\alpha v\beta 3$ activity[32]. Cyclo (-RGDfK) effectively inhibited HUVEC proliferation and viability and exhibited an IC50 value of 115.08 ng/mL (Fig. S5A). Next, we established PDTOs to further investigate the effects of DPP (Fig. S5G). Gene editing in PDTOs was performed to manipulate *DPP* and *DSP* expression, and successful generation of PDTOs overexpressing *DPP* and *DSP* was confirmed using immunofluorescence assays and Western blot analyses (Fig. 4L, Fig. S5I). Consistently, only the CM of *DPP*-overexpressing PDTOs significantly increased tubule formation in HUVECs, and this effect was reversed by cyclo (-RGDfK) (Fig. 4M and Fig. S5H and S5J).

3.5. DSPP/αvβ3/MAPK signaling axis promotes tumor vessel abnormalization

KEGG and WiKi pathway enrichment analyses indicated the essential role of DSPP in regulating tumor vasculature (Fig. 5A and B and Supporting Information Fig. S6A). Gene set enrichment analysis revealed enrichment of the mitogen-activated protein kinase (MAPK) signaling pathway in DSPP-overexpressing tissues (Fig. 5C). Moreover, the CM of *DSPP* overexpressing CRC cells could significantly increase p-ERK expression in HUVECs compared with the control, and $\alpha v\beta 3$ inhibition by cyclo (-RGDfK) and α-DSPP could attenuate the p-ERK upregulation (Fig. 5D). Selumetinib (AZD6244), a selective MAPK kinase inhibitor that blocks ERK signaling, effectively attenuated the DSPP-induced increase in tubule formation, thereby rescuing angiogenesis (Fig. 5E and F and Fig. S6B). We then employed real-time quantitative PCR to assess the expression of genes associated with vascular abnormalities. CRC-secreted DSPP could upregulate angiogenesis and matrix metalloproteinase family-related genes, and this effect was rescued by AZD6244 (Fig. 5G and H).

3.6. Interleukin-17 F (IL-17F) upregulates DSPP expression and induces vascular abnormalities in CRC

We investigated the effect of various inflammatory factors on *DSPP* expression in HCT8 cells. Treatment with IL-17F significantly increased *DSPP* expression (Fig. 6A). Real-time quantitative PCR and Western blot analyses revealed that IL-17F, but not IL-17A, elevated *DSPP* expression in HCT8 and HCT116 cells (Fig. 6B and C, Supporting Information Fig. S7A). However, IL-17F administration did not affect tubule formation in HUVECs (Fig. S7B). Meanwhile, both the CM of *DSPP* overexpressing HCT8 cells and IL-17F stimulated CRC cells enhanced angiogenesis. However, this stimulatory effect could be attenuated by α-DSPP, cyclo(-RGDfK), and AZD6244 (Fig. 6D and Fig. S7C). Additionally, neutralizing antibodies targeting interleukin-17 receptor A (IL-17RA) and interleukin-17 receptor C (IL-17RC) effectively reversed IL-17F-induced upregulation of DSPP expression (Fig. 6E). As IL-17F and IL-17RA/IL-17RC binding can activate downstream nuclear factor kappa-B (NF-κB) signaling, we confirmed the presence of a p65 binding site in the promoter region of *DSPP* using the JASPAR online database. Chromatin immunoprecipitation and luciferase reporter assays confirmed direct binding of p65 to the *DSPP* promoter region in both 293 T and HCT8 cells (Fig. 6F and G), and IL-17F could enhance the binding of p65 to the *DSPP* promoter and transcriptional activity of *DSPP* in HCT8 cells (Fig. 6I). Immunofluorescence staining revealed increased intracellular p65 phosphorylation in IL-17F-treated HCT8 cells (Fig. 6H). Western blot analyses indicated that DSPP could activate NF-κB signaling, whereas IL-17RA antibody or IκBα inhibitor BAY11-7082 attenuated the effect of DSPP (Fig. 6J and K).

The mediating role of DSPP in IL-17F-induced tumor growth (Fig. 6L and M, right panel and Fig. S7D), liver metastasis (Fig. 6M, left panel), and abnormal tumor vessel formation (Fig. 6N) was also investigated in an *in vivo* orthotopic transplantation model. Both α-DSPP and cyclo (-RGDfK) could reverse IL-17F effects on the orthotopic tumor growth, liver metastasis, hypoxia, vascular perfusion, and α-SMA$^+$ pericyte coverage (Fig. 6L−N).

3.7. DSPP is upregulated in CRC and associated with poor survival

Among the SIBLINGs, the expression of *DSPP* was significantly elevated in mCRC tissues (Fig. 7A and C, Supporting Information Table S2), whereas no significant differences were observed in the expression of BSP, DMP1, MEPE, and OPN (Supporting Information Fig. S8A). Moreover, our findings indicated a positive correlation between *DSPP* expression and an increased number of tortuous blood vessels (Fig. 7B). Analysis of the GSE39582 database revealed a positive correlation of *DSPP* expression with an increased risk of tumor lymph node involvement and advanced Duke's stage (Fig. 7D). *DSPP* expression was assessed in 12 paired CRC samples and corresponding adjacent normal tissue samples. A significantly higher *DSPP* expression was observed in CRC tissues, highlighting its potential role in cancer progression (Fig. 7E and Fig. S8B). Moreover, patients with mCRC exhibited significantly higher serum *DSPP* levels than healthy controls, reflecting a positive correlation between higher serum *DSPP* levels and patients with mCRC (Fig. 7F, Supporting Information Table S3). Additionally, Kaplan−Meier survival analysis demonstrated a close association between elevated DSPP levels and worse prognosis in patients with CRC (Fig. 7G). Multiplex

Luciferase reporter assay demonstrates IL-17F affects the interaction of p65 to the *DSPP* promoter. (J, K) Western blot assay shows the nuclear factor kappa-B (NF-κB) signaling pathway components expression. (L) *In vivo* bioluminescent images of orthotopic tumors in mice transplanted with the indicated HCT116 cells. (M) HE staining shows the metastasis of the orthotopic tumor in the liver and spleen. The quantification of the microvascular density is shown on the right. Scale bars = 100 μm. Data are presented as mean ± SD ($n = 4$). (N) Representative images of IF staining of orthotopic tumors, and the quantification of Hypoxyprobe$^+$ areas, dextran leakage, and lectin perfusion of orthotopic tumor vessels. Scale bar = 20 μm. Data are presented as mean ± SD ($n = 5$). *$P < 0.05$, **$P < 0.01$, ***$P < 0.001$; ns, no significance.

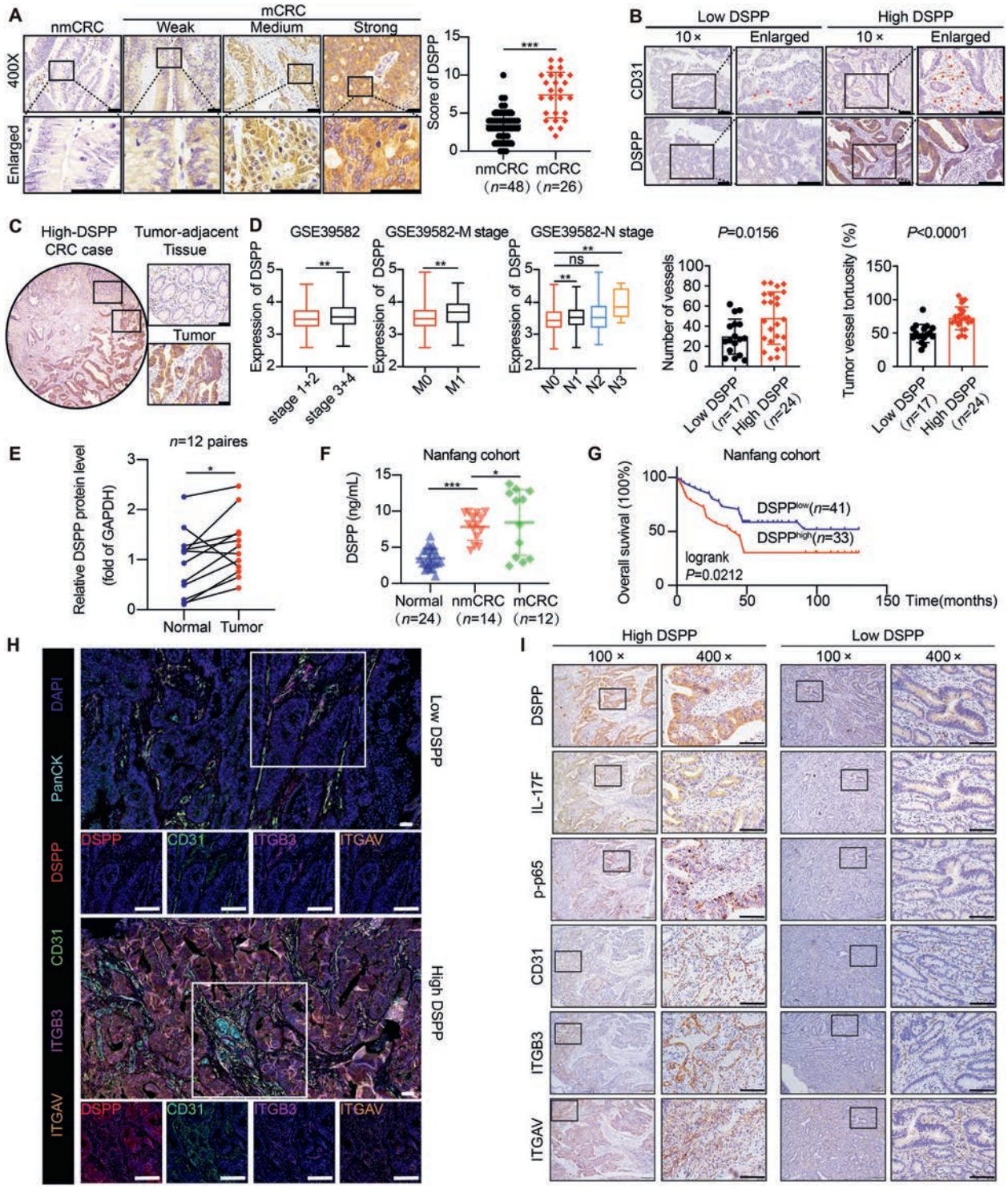

Figure 7 DSPP is upregulated in CRC and associated with poor survival. (A) Representative IHC images showing DSPP expression levels in CRC tissues compared to adjacent normal mucosa. Scale bar = 50 μm. The right panel presents quantified IHC scores of DSPP in CRC tissues along with paired adjacent normal tissues. (B) Representative CD31 IHC staining images of tumor tissue with low and high level of DSPP expression. Scale bar = 50 μm. The tumor vessel number and tortuousity in CRC tissues with low and high DSPP expression were quantified in the right panel. (C) Representative IHC images of a CRC patient with high DSPP expression in tumors but no expression in adjacent normal tissues. Scale bar = 50 μm. (D) The relationship between DSPP expression and tumor lymph node metastasis, as well as Duke's stage was detected by the GSE39582 database. (E) The graph shows the expression of *DSPP* normalized to *GAPDH* in 12 pairs of CRC tumor tissues and adjacent normal tissues. (F) Enzyme-linked immunosorbent assay analysis reveals the concentration of DSPP in serum from nmCRC and mCRC patients, compared to levels observed in healthy control individuals. (G) Kaplan−Meier survival analyses show the overall survival of 74 CRC patients based on DSPP expression. (H) The staining of DAPI, PanCK, DSPP, CD31, ITGB3, ITGAV was performed in CRC tissue samples using mIF. Scale bar = 50 μm. (I) IHC analysis of DSPP, IL-17F, p-p65, CD31, ITGB3, ITGAV in CRC tissue samples. Scale bar = 100 μm. $^{*}P < 0.05$, $^{**}P < 0.01$, $^{***}P < 0.001$; ns, no significance.

immunofluorescence staining revealed an increased number of tortuous blood vessels in CRC tissues with high *DSPP* expression (Fig. 7H). Furthermore, immunohistochemical analysis confirmed positive correlations between *DSPP* expression and the levels of IL-17F, phosphorylated p65 (p-p65), CD31, ITGAV, and ITGB3. Specifically, high *DSPP* expression was associated with elevated IL-17F, ITGAV, and ITGB3 levels, increased vascular abnormality, and enhanced intracellular p65 phosphorylation in CRC cells, whereas low *DSPP* expression exhibited the opposite pattern in CRC tissues (Fig. 7I).

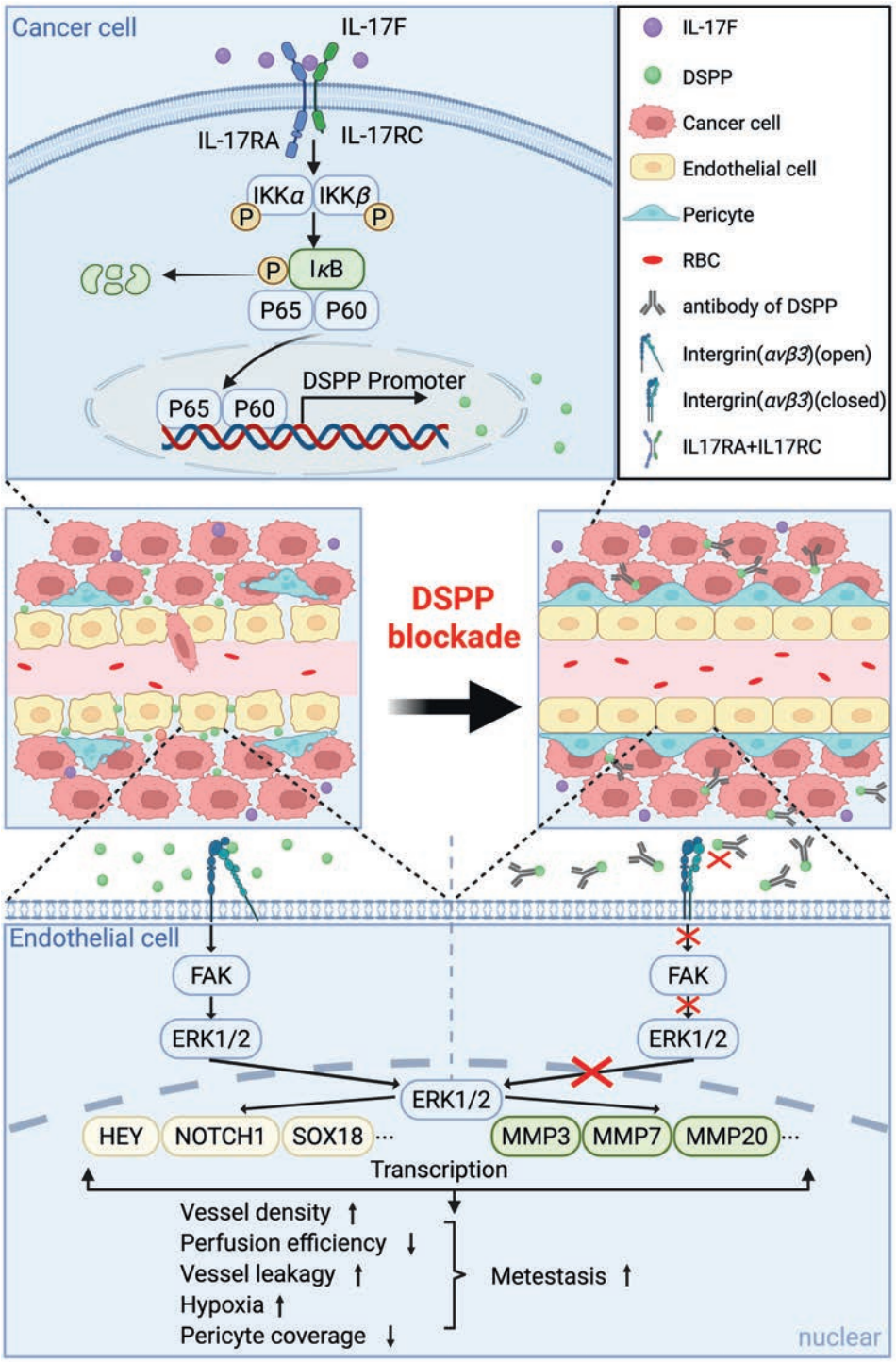

Figure 8 A schematic diagram shows the action mechanism of DSPP in regulating tumor vascular abnormalization to induce tumor metastasis. In the tumor microenvironment, IL-7F enhances the expression and secretion of DSPP in CRC. The CRC-secreted DSPP binds to the integrin $\alpha v\beta 3$ on the endothelial cell surface and activates the downstream FAK/MAPK signaling to induce tumor vascular abnormalization, finally promote tumor metastasis.

4. Discussion

TVN represents a promising strategy to enhance the efficacy of anticancer treatments. TVN improves tumor perfusion and oxygenation by restoring the structural and functional integrity of the abnormal tumor vasculature, thereby fostering a more favorable microenvironment for enhanced delivery and efficacy of chemotherapy, radiotherapy, and immunotherapy[5]. This approach shifts the paradigm from depriving tumors of nutrients through angiogenesis inhibition to reestablishing vascular function to combat tumor progression more effectively. Nevertheless, the precise molecular and cellular mechanisms underlying TVN remain unclear.

SIBLINGs are small soluble ligands that can bind to integrins through their RGD motifs, distinguishing them from large extracellular matrix proteins[16]. This interaction enables SIBLINGs to regulate tumor progression and angiogenesis. They influence EC behavior, which is crucial for the formation of new blood vessels[33]. OPN and BSP are linked to cancer metastasis[34]. DMP1 influences angiogenesis by inducing the membrane expression of VE-cadherin, a key component of EC junctions[35]. SIBLINGs can influence tumor growth and metastasis by modulating the angiogenic process, and understanding the specific mechanisms by which SIBLINGs regulate angiogenesis may provide insights into novel therapeutic strategies targeting these pathways to inhibit tumor vascularization and growth. As a member of SIBLINGs, DSPP is also implicated in malignant behaviors. Our findings revealed aberrantly elevated serum DSPP levels in patients with CRC, reflecting an association between DSPP and tumor vascular abnormalities leading to tumor metastasis.

Integrins are heterodimers composed of α and β subunits, each exhibiting distinct binding specificities and signaling properties, located at the cell surface[36]. Integrin $\alpha v\beta 3$, which specifically recognizes ligands with RGD motifs, is largely inactive in normal epithelial cells but is highly expressed and activated in tumor endothelial cells[37]. This integrin plays a critical role in tumor angiogenesis, migration, invasion, and metastasis, as well as in modulating inflammatory responses[38]. Therefore, targeting integrin $\alpha v\beta 3$ or its ligands holds great significance for tumor diagnosis and treatment.

Although OPN and BSP have been reported as pro-angiogenic factors, our study revealed that DSPP, *via* its cleaved form DPP, directly interacts with integrin $\alpha v\beta 3$[39−41]. In the present study, SPR and GST pull-down assays confirmed DSPP as a specific ligand of integrin $\alpha v\beta 3$, which binds to the extracellular peptide segments of ITGAV (1−438 amino acids) and ITGB3 (109−352 amino acids). Most integrins form complexes with extracellular matrix molecules and transmit signals to intracellular cytoskeletal proteins *via* their β subunits, thereby activating downstream signaling pathways[36]. Our study demonstrated that the interaction of tumor-secreted DSPP and integrin $\alpha v\beta 3$ on the EC surface could activate the Focal Adhesion Kinase (FAK)−MAPK pathway. Consistent with previous findings that blocking SIBLING-integrin interactions reduces angiogenesis and tumor growth[40], integrin-specific inhibitors significantly inhibited DSPP−$\alpha v\beta 3$ interaction and suppressed FAK−MAPK signaling in our study.

Inflammatory cytokines, including IL-6 and IL-8, can activate transcription factors such as NF-κB and signal transducer and activator of transcription 3 (STAT3), which can promote tumor angiogenesis by upregulating vascular endothelial growth factor expression[42,43]. C−C motif chemokine ligand 20, a macrophage-derived cytokine, upregulates DSPP expression in cancer cells[44]. Congruently, IL-17F promoted *DSPP* expression in tumor cells in a dose-dependent manner in our study (Fig. 6A−C and Fig. S7A). IL-17F belongs to the IL-17 family and shares approximately 50% amino acid sequence identity with IL-17A[45−47]. IL-17 signaling is linked to cell migration and invasion in multiple cancers, including oral squamous cell carcinoma[48], breast cancer[49], and gastric cancer[50]. For instance, IL-17A facilitates invasion, migration, and cancer stem cell-like properties by activating the STAT3/NF-κB signaling pathway[51]. IL-17A indirectly promotes tumor cell proliferation by enhancing blood vessel development within the tumor microenvironment, involving the secretion of pro-angiogenic factors and activation of matrix metalloproteinases in tumor cells, stromal endothelial cells, and fibroblasts, thereby improving nutrient availability to cancer cells[52,53]. Both IL-17A and IL-17F signal through the receptors IL-17RA and IL-17RC, forming a heteromeric complex that mediates downstream signaling[54]. Despite the established significance of IL-17A, IL-17F plays a complex and context-dependent role in CRC. IL-17F promotes the self-renewal of cancer-initiating cells in CRC and ovarian cancer, indicating its potential role in maintaining cancer stem cell populations[55]. Moreover, IL-17F may promote tumor growth and progression[56].

The present study revealed that IL-17F promotes *DSPP* expression in CRC cells. Mechanistically, IL-17F-mediated *DSPP* upregulation can be counteracted by antibodies targeting the IL-17RA and IL-17RC receptors. IL-17 induces the expression of IκBζ, a key transcriptional regulator, in the NF-κB signaling pathway through both transcriptional and translational induction, which enhances mRNA and protein synthesis of numerous target genes of NF-κB[57−60]. Meanwhile, the promoter regions of SIBLINGs contain regulatory sequences with potential binding sites for transcription factors, including activator protein-1 and NF-κB, which are involved in processes such as inflammation and tumorigenesis[16]. Our findings revealed that IL-17F activates the NF-κB signaling pathway, enhancing p65 binding to the *DSPP* promoter region, thereby upregulating *DSPP* expression.

5. Conclusions

The present study highlights a close relationship between vascular abnormalities and metastasis in CRC. We identified DSPP as a critical mediator of tumor vascular dysfunction and metastasis, highlighting it as a potential therapeutic target. Mechanistically, IL-17F upregulates *DSPP* expression and secretion in CRC cells in the inflammatory tumor microenvironment. Subsequently, secreted DSPP activates downstream FAK−MAPK signaling by binding to integrin $\alpha v\beta 3$ on the EC surface, thus promoting tumor vascular abnormalization and metastasis (Fig. 8). Overall, our study provides robust evidence that DSPP is a novel predictive biomarker for TVN and metastasis, offering a promising avenue for therapeutic interventions in CRC.

Acknowledgements

This research was supported by grants from the National Science and Technology Major Project (2023ZD0500103, China), the National Natural Science Foundation of China (81972813, 82103393, 82472895, 82403601), Guangdong Basic and Applied Basic Research Foundation (2022A151511088, 2023A1515011991, 2024A1515030276, China), and China Postdoctoral Science Foundation (2023M741569).

Author contributions

Chaoqun Liu: Investigation; methodology. Rui Zhou: Project administration; writing-review and editing. Weiwei Liu:

Investigation; methodology. Rui Li: Resources; visualization. Jun Xiao: Resources; visualization. Jianghua Wu: Methodology. Ziyan Ning: Methodology. Zilin Chen: Methodology. Chen Qian: Data curation. Yujie Zhang: Data curation. Wandie Lin: Formal analysis. Liang Zhao: Conceptualization; supervision; writing-review and editing.

Conflicts of interest

The authors declare no potential conflicts of interest.

Appendix A. Supporting information

Supporting information to this article can be found online at https://doi.org/10.1016/j.apsb.2026.06.011.

References

1. Siegel RL, Giaquinto AN, Jemal A. Cancer statistics, 2024. *CA Cancer J Clin* 2024;**74**:12−49.
2. Ciardiello F, Ciardiello D, Martini G, Napolitano S, Tabernero J, Cervantes A. Clinical management of metastatic colorectal cancer in the era of precision medicine. *CA Cancer J Clin* 2022;**72**:372−401.
3. Dekker E, Tanis PJ, Vleugels JLA, Kasi PM, Wallace MB. Colorectal cancer. *Lancet* 2019;**394**:1467−80.
4. De Falco V, Napolitano S, Rosello S, Huerta M, Cervantes A, Ciardiello F, et al. How we treat metastatic colorectal cancer. *ESMO Open* 2020;**4**:e000813.
5. Jain RK. Antiangiogenesis strategies revisited: from starving tumors to alleviating hypoxia. *Cancer Cell* 2014;**26**:605−22.
6. Carmeliet P, Jain RK. Principles and mechanisms of vessel normalization for cancer and other angiogenic diseases. *Nat Rev Drug Discov* 2011;**10**:417−27.
7. Hanahan D, Weinberg RA. Hallmarks of cancer: the next generation. *Cell* 2011;**144**:646−74.
8. Nagy JA, Chang SH, Shih SC, Dvorak AM, Dvorak HF. Heterogeneity of the tumor vasculature. *Semin Thromb Hemost* 2010;**36**:321−31.
9. Kim C, Yang H, Fukushima Y, Saw PE, Lee J, Park JS, et al. Vascular RhoJ is an effective and selective target for tumor angiogenesis and vascular disruption. *Cancer Cell* 2014;**25**:102−17.
10. Cantelmo AR, Conradi LC, Brajic A, Goveia J, Kalucka J, Pircher A, et al. Inhibition of the glycolytic activator PFKFB3 in endothelium induces tumor vessel normalization, impairs metastasis, and improves chemotherapy. *Cancer Cell* 2016;**30**:968−85.
11. Martin JD, Seano G, Jain RK. Normalizing function of tumor vessels: progress, opportunities, and challenges. *Annu Rev Physiol* 2019;**81**: 505−34.
12. Johansson-Percival A, He B, Li ZJ, Kjellen A, Russell K, Li J, et al. *De novo* induction of intratumoral lymphoid structures and vessel normalization enhances immunotherapy in resistant tumors. *Nat Immunol* 2017;**18**:1207−17.
13. Wang W, Li T, Cheng Y, Li F, Qi S, Mao M, et al. Identification of hypoxic macrophages in glioblastoma with therapeutic potential for vasculature normalization. *Cancer Cell* 2024;**42**:815-32.e12.
14. Rahbari NN, Kedrin D, Incio J, Liu H, Ho WW, Nia HT, et al. Anti-VEGF therapy induces ECM remodeling and mechanical barriers to therapy in colorectal cancer liver metastases. *Sci Transl Med* 2016;**8**: 360ra135.
15. Jung K, Heishi T, Khan OF, Kowalski PS, Incio J, Rahbari NN, et al. Ly6Clo monocytes drive immunosuppression and confer resistance to anti-VEGFR2 cancer therapy. *J Clin Investig* 2017;**127**:3039−51.
16. Bellahcene A, Castronovo V, Ogbureke KU, Fisher LW, Fedarko NS. Small integrin-binding ligand *N*-linked glycoproteins (SIBLINGs): multifunctional proteins in cancer. *Nat Rev Cancer* 2008;**8**:212−26.
17. Hayashi C, Rittling S, Hayata T, Amagasa T, Denhardt D, Ezura Y, et al. Serum osteopontin, an enhancer of tumor metastasis to bone, promotes B16 melanoma cell migration. *J Cell Biochem* 2007;**101**:979−86.
18. Veis A, Perry A. The phosphoprotein of the dentin matrix. *Biochemistry* 1967;**6**:2409−16.
19. Xiao S, Yu C, Chou X, Yuan W, Wang Y, Bu L, et al. Dentinogenesis imperfecta 1 with or without progressive hearing loss is associated with distinct mutations in DSPP. *Nat Genet* 2001;**27**:201−4.
20. Zhang X, Zhao J, Li C, Gao S, Qiu C, Liu P, et al. DSPP mutation in dentinogenesis imperfecta shields type II. *Nat Genet* 2001;**27**:151−2.
21. Aseervatham J, Ogbureke KUE. Effects of DSPP and MMP20 silencing on adhesion, metastasis, angiogenesis, and epithelial−mesenchymal transition proteins in oral squamous cell carcinoma cells. *Int J Mol Sci* 2020;**21**:4734.
22. Nikitakis NG, Gkouveris I, Aseervatham J, Barahona K, Ogbureke KUE. *DSPP-MMP20* gene silencing downregulates cancer stem cell markers in human oral cancer cells. *Cell Mol Biol Lett* 2018; **23**:30.
23. Gkouveris I, Nikitakis NG, Aseervatham J, Ogbureke KUE. The tumorigenic role of DSPP and its potential regulation of the unfolded protein response and ER stress in oral cancer cells. *Int J Oncol* 2018; **53**:1743−51.
24. Joshi R, Tawfik A, Edeh N, McCloud V, Looney S, Lewis J, et al. Dentin sialophosphoprotein (*DSPP*) gene-silencing inhibits key tumorigenic activities in human oral cancer cell line, OSC2. *PLoS One* 2010;**5**:e13974.
25. Ogbureke KU, Abdelsayed RA, Kushner H, Li L, Fisher LW. Two members of the SIBLING family of proteins, DSPP and BSP, may predict the transition of oral epithelial dysplasia to oral squamous cell carcinoma. *Cancer* 2010;**116**:1709−17.
26. Faraji SN, Nejatollahi F, Tamaddon AM, Mohammadi M, Aminsharifi AR. Generation and characterization of a specific single-chain antibody against DSPP as a prostate cancer biomarker: involvement of bioinformatics-based design of novel epitopes. *Int Immunopharmacol* 2019;**69**:217−24.
27. Chaplet M, Waltregny D, Detry C, Fisher LW, Castronovo V, Bellahcene A. Expression of dentin sialophosphoprotein in human prostate cancer and its correlation with tumor aggressiveness. *Int J Cancer* 2006;**118**:850−6.
28. Fan S, Gao H, Sun L, Zhu F, Zhou R, Zhang W, et al. Knockdown of DSPP inhibits the migration and invasion of glioma cells. *Pathol Res Pract* 2018;**214**:2025−30.
29. Liu C, Pan Z, Chen Q, Chen Z, Liu W, Wu L, et al. Pharmacological targeting PTK6 inhibits the JAK2/STAT3 sustained stemness and reverses chemoresistance of colorectal cancer. *J Exp Clin Cancer Res* 2021;**40**:297.
30. Schmitt M, Ceteci F, Gupta J, Pesic M, Bottger TW, Nicolas AM, et al. Colon tumour cell death causes mTOR dependence by paracrine P2X4 stimulation. *Nature* 2022;**612**:347−53.
31. Zhang Y, Zhao W, Wu L, Ai T, He J, Chen Z, et al. Inhibition of CCT5-mediated asparagine biosynthesis and anti-PD-L1 produce synergistic antitumor effects in colorectal cancer. *Acta Pharm Sin B* 2025;**15**:2480−97.
32. Simecek J, Notni J, Kapp TG, Kessler H, Wester HJ. Benefits of NOPO as chelator in gallium-68 peptides, exemplified by preclinical characterization of ^{68}Ga-NOPO-c(RGDfK). *Mol Pharm* 2014;**11**: 1687−95.
33. Lamour V, Nokin MJ, Henry A, Castronovo V, Bellahcene A. SIBLING proteins: molecular tools for tumor progression and angiogenesis. *Med Sci* 2013;**29**:1018−25.
34. Ibrahim T, Leong I, Sanchez-Sweatman O, Khokha R, Sodek J, Tenenbaum HC, et al. Expression of bone sialoprotein and osteopontin in breast cancer bone metastases. *Clin Exp Metastasis* 2000;**18**:253−60.
35. Pirotte S, Lamour V, Lambert V, Alvarez Gonzalez ML, Ormenese S, Noel A, et al. Dentin matrix protein 1 induces membrane expression of VE-cadherin on endothelial cells and inhibits VEGF-induced angiogenesis by blocking VEGFR-2 phosphorylation. *Blood* 2011;**117**: 2515−26.

36. Giancotti FG, Ruoslahti E. Integrin signaling. *Science* 1999;**285**: 1028−32.
37. Brooks PC, Clark RA, Cheresh DA. Requirement of vascular integrin alpha v beta 3 for angiogenesis. *Science* 1994;**264**:569−71.
38. Desgrosellier JS, Cheresh DA. Integrins in cancer: biological implications and therapeutic opportunities. *Nat Rev Cancer* 2010;**10**:9−22.
39. Tang H, Wang J, Bai F, Hong L, Liang J, Gao J, et al. Inhibition of osteopontin would suppress angiogenesis in gastric cancer. *Biochem Cell Biol* 2007;**85**:103−10.
40. Chakraborty G, Jain S, Kundu GC. Osteopontin promotes vascular endothelial growth factor-dependent breast tumor growth and angiogenesis *via* autocrine and paracrine mechanisms. *Cancer Res* 2008;**68**: 152−61.
41. Baluk P, Morikawa S, Haskell A, Mancuso M, McDonald DM. Abnormalities of basement membrane on blood vessels and endothelial sprouts in tumors. *Am J Pathol* 2003;**163**:1801−15.
42. Mbeunkui F, Johann Jr DJ. Cancer and the tumor microenvironment: a review of an essential relationship. *Cancer Chemother Pharmacol* 2009;**63**:571−82.
43. Li D, Xie K, Ding G, Li J, Chen K, Li H, et al. Tumor resistance to anti-VEGF therapy through up-regulation of VEGF-C expression. *Cancer Lett* 2014;**346**:45−52.
44. Shiba H, Mouri Y, Komatsuzawa H, Ouhara K, Takeda K, Sugai M, et al. Macrophage inflammatory protein-3 alpha and beta-defensin-2 stimulate dentin sialophosphoprotein gene expression in human pulp cells. *Biochem Biophys Res Commun* 2003;**306**:867−71.
45. Bettelli E, Carrier Y, Gao W, Korn T, Strom TB, Oukka M, et al. Reciprocal developmental pathways for the generation of pathogenic effector TH17 and regulatory T cells. *Nature* 2006;**441**:235−8.
46. Harrington LE, Hatton RD, Mangan PR, Turner H, Murphy TL, Murphy KM, et al. Interleukin 17-producing $CD4^+$ effector T cells develop *via* a lineage distinct from the T helper type 1 and 2 lineages. *Nat Immunol* 2005;**6**:1123−32.
47. Park H, Li Z, Yang XO, Chang SH, Nurieva R, Wang YH, et al. A distinct lineage of CD4 T cells regulates tissue inflammation by producing interleukin 17. *Nat Immunol* 2005;**6**:1133−41.
48. Zhang S, Wang X, Gupta A, Fang X, Wang L, Zhang C. Expression of IL-17 with tumor budding as a prognostic marker in oral squamous cell carcinoma. *Am J Transl Res* 2019;**11**:1876−83.
49. Zhu X, Mulcahy LA, Mohammed RA, Lee AH, Franks HA, Kilpatrick L, et al. IL-17 expression by breast-cancer-associated macrophages: IL-17 promotes invasiveness of breast cancer cell lines. *Breast Cancer Res* 2008;**10**:R95.
50. Wang T, Zhang J, Cui L. Apatinib inhibits gastric carcinoma development by regulating the expression levels of IL-17 *via* the Bax/Bcl-2 signaling pathway. *Exp Ther Med* 2021;**21**:654.
51. Fu X, Hong L, Yang Z, Tu Y, Xin W, Zha M, et al. MicroRNA-148a-3p suppresses epithelial-to-mesenchymal transition and stemness properties *via* Wnt1-mediated Wnt/beta-catenin pathway in pancreatic cancer. *J Cell Mol Med* 2020;**24**:13020−35.
52. Wu F, Xu J, Huang Q, Han J, Duan L, Fan J, et al. The role of Interleukin-17 in lung cancer. *Mediat Inflamm* 2016;**2016**:8494079.
53. Huang Q, Duan L, Qian X, Fan J, Lv Z, Zhang X, et al. IL-17 promotes angiogenic factors IL-6, IL-8, and Vegf production *via* Stat 1 in lung adenocarcinoma. *Sci Rep* 2016;**6**:36551.
54. Wright JF, Bennett F, Li B, Brooks J, Luxenberg DP, Whitters MJ, et al. The human IL-17F/IL-17A heterodimeric cytokine signals through the IL-17RA/IL-17RC receptor complex. *J Immunol* 2008;**181**:2799−805.
55. Zhao J, Chen X, Herjan T, Li X. The role of interleukin-17 in tumor development and progression. *J Exp Med* 2020;**217**:e20190297.
56. Mikkola T, Almahmoudi R, Salo T, Al-Samadi A. Variable roles of interleukin-17F in different cancers. *BMC Cancer* 2022;**22**:54.
57. Karlsen JR, Borregaard N, Cowland JB. Induction of neutrophil gelatinase-associated lipocalin expression by co-stimulation with interleukin-17 and tumor necrosis factor-alpha is controlled by IkappaB-zeta but neither by C/EBP-beta nor C/EBP-delta. *J Biol Chem* 2010;**285**:14088−100.
58. Zhu S, Pan W, Song X, Liu Y, Shao X, Tang Y, et al. The microRNA miR-23b suppresses IL-17-associated autoimmune inflammation by targeting TAB2, TAB3 and IKK-alpha. *Nat Med* 2012;**18**:1077−86.
59. Yamazaki S, Muta T, Matsuo S, Takeshige K. Stimulus-specific induction of a novel nuclear factor-kappaB regulator, IkappaB-zeta, *via* Toll/interleukin-1 receptor is mediated by mRNA stabilization. *J Biol Chem* 2005;**280**:1678−87.
60. Shen F, Ruddy MJ, Plamondon P, Gaffen SL. Cytokines link osteoblasts and inflammation: microarray analysis of interleukin-17- and TNF-alpha-induced genes in bone cells. *J Leukoc Biol* 2005;**77**:388−99.